

1 **Modelling groundwater recharge, actual evaporation and** 2 **transpiration in semi-arid sites of the Lake Chad Basin: The role of** 3 **soil and vegetation on groundwater recharge**

4 Christoph Neukum¹, Angela Gabriela Morales Santos², Melanie Ronelngar³, Aminu Bala⁴, Sara Ines
5 Vassolo¹

6 ¹ Federal Institute for Geosciences and Natural Resources, Department of Groundwater and Soil, Stilleweg 2, 30655 Hannover,
7 Germany

8 ² University of Natural Resources and Life Sciences, Vienna, Department of Water, Atmosphere and Environment, Institute
9 for Soil Physics and Rural Water Management, Muthgasse 18, 1190 Vienna, Austria

10 ³ Federal Institute for Geosciences and Natural Resources at Lake Chad Basin Commission, Rond Point des Armes, Ndjamena,
11 Chad

12 ⁴ Lake Chad Basin Commission, Rond Point des Armes, Ndjamena, Chad

13 *Correspondence to:* Christoph Neukum (christoph.neukum@bgr.de)

14 **Abstract**

15 The Lake Chad Basin, located in the center of North Africa, is characterized by strong climate seasonality with a pronounced
16 short annual precipitation period and high potential evapotranspiration. Groundwater is an essential source for drinking water
17 supply as well as for agriculture and groundwater related ecosystems. Thus, assessment of groundwater recharge is very
18 important although difficult, because of the strong effects of evaporation and transpiration as well as limited available data.

19 A simple, generalized approach, which requires only limited field data, freely available remote sensing data as well as well-
20 established concepts and models, is tested for assessing groundwater recharge in the southern part of the basin. This work uses
21 the FAO-dual K_c concept to estimate E and T coefficients at six locations that differ in soil texture, climate, and vegetation
22 conditions. Measured values of soil water content and chloride concentrations along vertical soil profiles together with different
23 scenarios for E and T partitioning and a Bayesian calibration approach are used to numerically simulate water flow and chloride
24 transport using Hydrus-1D. Average groundwater recharge rates and the associated model uncertainty at the six locations are
25 assessed for the 2003-2016 time-period.

26 Annual groundwater recharge varies between 6 and 93 mm and depends strongly on soil texture and related water retention
27 and on vegetation. Interannual variability of groundwater recharge is generally greater than the uncertainty of the simulated
28 groundwater recharge.

29 **1 Introduction**

30 Recharge occurs even in the most arid regions, mainly due to concentration of surface flow and ponding with lateral and
31 vertical infiltration (Lloyd, 1986). Direct recharge by precipitation is possible in semi-arid regions, but intermittently, owing
32 to the fluctuations in the periodicity and volume of precipitation that is inherent to such regions (Lloyd, 2009). Scanlon et al.

33 (2006) synthesized recharge estimates for semiarid and arid regions worldwide. They found that recharge is sensitive to land
34 use and cover changes, hence management of such changes are necessary to control recharge. Moreover, they stated that
35 average recharge rates in semi-arid and arid regions range from 0.2 to 35 mm yr⁻¹, representing 0.1 to 5% of long-term average
36 annual precipitation. Recently, Cuthbert et al. (2019) investigated the relationship between precipitation and recharge in sub-
37 Saharan Africa using multidecadal hydrographs. They found that focused recharge predominates in arid areas and is mainly
38 controlled by intense rainfall and flooding events. Intense precipitation, even during years of low annual precipitation, results
39 in some of the most significant years of recharge in dry subtropical locations.

40 The arid to semi-arid Lake Chad Basin (LCB) is one of the largest endorheic basins of the world with an area of approximately
41 2.5 million km². It covers parts of Algeria, Cameroon, Central African Republic, Chad, Libya, Niger, Nigeria, and Sudan.
42 According to the Lake Chad Basin Commission (LCBC, 2012), 45 million inhabitants are settled in the basin. The study areas
43 of Salamat and Waza Logone are located in the southern part of the LCB along the Chari-Logone, the major tributary river
44 system to Lake Chad (Figure 1), which accounts for around 80-90% of the inflow to the Lake Chad (Bouchez et al., 2016).

45 Groundwater is an important source for drinking water supply as well as for agriculture and groundwater related ecosystems
46 in the LCB. Lake Chad, associated rivers, and the floodplains of the major rivers are characterized by strong seasonality, due
47 to a pronounced short annual precipitation period and high potential evapotranspiration. Groundwater recharge, evaporation,
48 transpiration, and the entire hydrological budget depend strongly on seasonality. However, the impact of transpiration as a
49 potentially significant process of the hydrological budget (Jasechko et al., 2013) has not yet been intensively explored in the
50 region (Bouchez et al., 2016).

51 Many studies have been published concerning the hydrological behaviour and budget of Lake Chad, due to its substantial and
52 frequent open water surface changes and related consequences to the population and the environment (e.g. Bouchez et al.,
53 2016; Lemoalle et al., 2014; Lemoalle et al., 2012; Olivry et al., 1996; Vuillaume, 1981). Another important topic associated
54 to Lake Chad is groundwater recharge by infiltration of lake water into the Quaternary aquifer, which was estimated by isotope
55 studies (Fontes et al., 1969; Fontes et al., 1970; Zairi, 2008), water and salt budgets (Bouchez et al., 2016; Bader et al., 2011;
56 Carmouze, 1972; Roche, 1980), and hydrogeological models (Isihoro et al., 1996; Leblanc, 2002).

57 Very significant for an arid to semi-arid region is the determination of diffuse groundwater recharge, evaporation of surface
58 and soil water as well as transpiration from plants. In the LCB, recharge has been assessed using different methods. The
59 Chloride Mass Balance (CMB) approach is a widely used technique. Edmunds and Gaye (1994) used interstitial water chloride
60 profiles from the unsaturated zone, in combination with measurements of chemical parameters from dug well samples, to
61 calculate groundwater recharge in the Sahel. They estimated a recharge rate of 13 mm year⁻¹ for a mean annual rainfall from
62 1970-1990 at 280 mm in their study area and concluded that it is an inexpensive technique, which can be applied in many arid
63 and semi-arid areas. Applying the same method, Edmunds et al. (2002) estimated direct recharge rates from precipitation in
64 the Manga Grasslands in NE Nigeria (western LCB) at rates between 16 mm year⁻¹ and 30 mm yr⁻¹. Including Cl values from
65 dug-wells, they appraised the regional direct recharge for north Nigeria at 43 mm year⁻¹, which highlights the importance of
66 infiltration from precipitation to the groundwater table at the regional scale. Tewelde et al. (2019) applied the CMB on soil

67 profiles of the LCB, which are partly used in this study. They estimated generally lower annual recharge in Salamat (3 to
68 111 mm year⁻¹) compared to Waza Logone (117 to 163 mm year⁻¹), whereas very low values were found for Bahr el Ghazal
69 (0.2 to 0.8 mm year⁻¹) and the northern pool of the Lake Chad (0.6 to 0.8 mm year⁻¹). They conclude that one major difficulty
70 of CMB is the choice of a representative chloride concentration, or the concentration that prevails at greater depths, when
71 evapotranspiration effects are negligible, particularly for soils with a strong vertical variability in chloride concentrations.
72 Recharge has also been assessed using groundwater modelling in the LCB (Eberschweiler, 1993; Massuel, 2001; Leblanc,
73 2002; Boronina et al., 2005; Vaquero et al., 2021), where diffused recharge has been obtained in the process of model
74 calibration. Calculated values differ considerably, depending on the vertical accuracy of the model and the extension of the
75 modelled area. It is also possible to determine recharge with the help of isotopes. Goni et al. (2021) used environmental isotopes
76 to conclude that recharge in the southwestern part of the LCB is mainly the result of strong precipitation events in the middle
77 of the wet season. Using the Cl³⁶ to Cl ratio, Bouchez et al. (2019) estimated a recharge rate of 240 ± 170 mm year⁻¹ for the
78 humid part of the LCB in the south. Recharge rates reduce to 78 ± 7 mm year⁻¹ for areas close to surface water and to 16 ± 27
79 mm year⁻¹ for regions unconnected to the hydrological network in the Sahelian part.

80 Concerning evaporation and transpiration, they were assessed for the Lake Chad coupling hydrological, chemical, and isotopic
81 models (Bouchez et al., 2016). They conclude, that evaporation varies from 2070 ± 100 mm year⁻¹ in the southern to 2270
82 ± 100 mm year⁻¹ in the northern pool, whereas transpiration is insignificant with an average of 300 mm year⁻¹ in the lake that
83 increases slightly to 500 mm year⁻¹ in the archipelagos, where vegetation is abundant. Furthermore, they state that their work
84 estimates transpiration of the Lake Chad for the first time. However, studies on evaporation and transpiration in the vadose
85 zone are largely missing in the LCB.

86 For vadose zone studies, partitioning evapotranspiration (ET) into its respective soil evaporation (E) and plant transpiration
87 (T) components is crucial for process-based understanding of fluxes (Anderson et al., 2017). There are a number of
88 measurement and modelling approaches that can be used to estimate E and T separately, including micro-lysimeters, soil heat
89 pulse probes, Bowen ratios, and Eddy covariance to determine E, and sap flow, chambers, and biomass-transpiration
90 relationships to measure T (Kool et al., 2014). Evapotranspiration partitioning can also be estimated directly by using stable
91 isotopes to assess the ratio between E and T (Wu et al. 2016). Stable isotopes were also used in combination with Eddy
92 covariance on semi-arid environments (Aouade et al., 2016).

93 The Food and Agricultural Organization of the United Nations (FAO) published a model (Allen et al., 1998) that uses an
94 empirically defined crop coefficient (K_c) in combination with a grass-reference potential ET (ET₀) to calculate crop potential
95 evapotranspiration (ET_c). There are two approaches for this method: single coefficient and dual crop coefficient. The FAO-
96 dual K_c model is a validated method for ET partitioning and the most commonly applied (Kool et al., 2014). It has been widely
97 used with good results for numerous crops under different conditions: e.g. wheat and maize in semi-arid regions (Shahrokhnia
98 and Sepaskhah, 2013), wheat in humid climates (Vieira et al., 2016), cherry trees in temperate continental monsoon climates
99 (Tong et al., 2016), and irrigated eucalyptus (Alves et al., 2013) and canola in terrestrial climates (Majnooni-Heris et al., 2012).

100 Quantification of water fluxes in the vadose zone and linking atmospheric water and solute input at the upper boundary of the
101 soil with water and solute fluxes at different soil depths is frequently implemented using different type of models. Numerical
102 models need information on vadose zone properties for accurate parametrization to link fluxes with state variables such as
103 unsaturated hydraulic conductivity and the water retention curve. Estimation of effective soil hydraulic parameters, which are
104 valid at the modelling scale, might be laborious. Furthermore, parameter estimation might vary significantly depending on the
105 measurement method (Mertens et al., 2005), when water and solute fluxes dynamics are considered. Hydraulic and transport
106 parameters obtained from inverse modelling can be ambiguous, if multiple parameters are simultaneously considered and
107 boundary conditions are not well known. Combining different state variables of water flow and solute transport in one objective
108 function was found to be a useful strategy for appropriate parametrization (Groh et al., 2018; Sprenger et al., 2015) and for the
109 transient simulation of water and solute fluxes. However, large amount of data are necessary to obtain accurate estimates of
110 state variables, which are rarely available in remote areas of Africa, and measurement of related variables are associated with
111 a huge effort in such environments. Pedotransfer functions (PTF) bridge available and needed data. They are frequently used
112 to quantify soil parameters (van Looy et al., 2017; Vereecken et al., 2016). PTF strive to provide a balance between data
113 accuracy and availability (Vereecken et al., 2016). Since PTF usually do not consider soil structure, their results are better for
114 homogeneous soils than for structured ones (Sprenger et al., 2015; Vereecken et al., 2010).

115 In general, time series of relevant data for estimating groundwater recharge is scarce in the LCB. A simple, generalized
116 approach, which requires only limited field data, freely available remote sensing data, and well-established concepts and
117 models, is tested for assessing groundwater recharge in the semi-arid part of the LCB. This work applies the FAO-dual K_c
118 concept to estimate E and T coefficients at six locations, which differ in soil texture, climate, and vegetation conditions.
119 Measured values of soil water content and chloride concentrations along vertical soil profiles, partly published by Tewelde et
120 al. (2019), together with different scenarios for E and T partitioning and a Bayesian calibration approach are used to
121 numerically simulate water flow and chloride transport as well as to produce time series of recharge. Both measured soil-
122 moisture and chloride concentrations are necessary for model calibration in order to get reliable estimates for water flow and
123 solute transport. Average potential groundwater recharge and the associated model uncertainty are assessed for the 2003-2016
124 time-period. This generalized method is applied to selected sites for estimating recharge in areas with low accessibility, but
125 cannot be extrapolated to the whole LCB.

126 **2 Data and methods**

127 **2.1 Study sites**

128 The LCB is a Mesozoic basin and a major part of its geology comprises sedimentary formations from the Tertiary and
129 Quaternary periods (LCBC, 1993). The Quaternary sediments form a continuous layer of fluvial, lacustrine and aeolian
130 sands. These medium to fine-grained sands act as an unconfined transboundary aquifer, as do all aquifers in the LCB, and are
131 isolated from underlying aquifers by a thick layer of Pliocene clay (Leblanc et al., 2007; Vassolo, 2009). The Tertiary formation

132 (Continental Terminal) consists of sandstones and argillaceous sands and is a classic example of a confined aquifer system
133 that becomes artesian in the surroundings of Lake Chad (Ngatcha et al., 2008). The availability of water from precipitation as
134 well as the deposition characteristics of the aquifer play an important role in the recharge of the upper unconfined sands
135 (Vassolo, 2009).

136 The study sites (Figure 1, Table 1) are located in the Salamat and Waza Logone floodplains in the southern Sahel zone.
137 Selection of sites was limited mainly by accessibility and project's goals. The sites correspond to those published by Tewelde
138 et al. (2019) for these areas, except for site ST4. Site ST4 is located far from any floodplain, which is the focus of this research,
139 and its soil composition and vegetation are very similar to those from site ST3. Thus, including this location would not provide
140 any additional information.

141 The types of soils included in the selected sites are sand, loam, clay, and their combinations, which are the most common in
142 the LCB. However, they surely do not cover all existent soils, due to the extension of the LCB. Sites ST1 and ST2 in Salamat
143 as well as WL1 and WL3 in Waza Logone are annually flooded over three months, site WL2 located at the edge of the Waza
144 Logone wetland is flooded only one month per year whereas site ST3, although close to ST1 in Salamat, is never flooded. In
145 the Salamat region, mainly sorghum is grown with trees such as *Acacia albida*, *A. scorpioides* and *A. sieberana*, present along
146 the margins of the floodplains (Bernacsek et al., 1992). In the Waza Logone area, vegetation depends on the duration of
147 submersion, forming grass savannahs that are flooded for longer periods of time (Batello et al., 2004). The selected sites cover
148 thus, the most common vegetation in the LCB. *Acacia* and grass are the most widespread natural vegetation, whereas sorghum
149 is the most commonly planted corn. Cotton, which is also planted, is only locally produced and generally using irrigation.
150 Mango trees can be found along the Chari and Logone rivers, but are not representative for the whole basin.

151 **2.2 Climate data**

152 Monthly precipitation and potential evapotranspiration data from 1970 to 2019 for the study sites were extracted from the
153 CRUTS 4 database (Harris et al., 2020). The potential evapotranspiration was calculated using the Penman-Monteith method
154 and is considered herein as the reference evapotranspiration (ET_0). Wind speeds at 10 m above ground for Salamat and Waza
155 Logone were obtained from Didane et al. (2017). To adjust these values for 2 m above ground, a correction factor of 0.7479
156 was applied, based on a logarithmic wind speed profile (Allen et al., 1998).

157 Average annual precipitation in Salamat and Waza Logone are 807 mm and 709 mm, respectively. The rainy season is typically
158 from May to September with maximum precipitation in July and August. Average annual values of ET_0 are 1718 mm in
159 Salamat and 2011 mm in Waza Logone, exceeding annual precipitation by more than a factor of 2. However, in the second
160 half of the rainy season, the monthly water balance is positive. The average water balance for July until September between
161 2003 and 2016 was $131 \pm 101 \text{ mm month}^{-1}$ and $90 \pm 63 \text{ mm month}^{-1}$ for Salamat and Waza Logone, respectively (Figure 2).

162 Chloride concentration was analyzed in the BGR laboratory in Hanover, Germany using a Thermo Fischer (Dionex) type ICS-
163 5000 ion chromatograph with a detection limit of 0.003 mg l^{-1} . Concentration in ponding water was measured in four samples
164 in Salamat, which varied between 2.5 mg l^{-1} and 25 mg l^{-1} .

165 Precipitation was sampled using a Hellmann rainwater collector in N'Djamena. This device was designed to minimize to a
166 minimum evaporation by using a narrow soft polypropylene plastic tube of 4 mm inner diameter to connect the funnel on top
167 of the device with the bottom of the 3 l collection bottle (Gröning et al., 2012). Once precipitation starts, water rises in the
168 bottle and into the tube decoupling the atmosphere from the bottle headspace to prevent evaporation. To ensure that evaporation
169 is as low as possible, sampling took place event-wise. Chloride concentration in precipitation was measured in 59 out of 147
170 samples collected in N'Djamena between 2014 and 2020 for different precipitation events and stages of the rainy season (Table
171 S1). Not all rain samples could be analyzed for chloride concentration, due to limited sample volume in minor events at the
172 beginning and end of the rainy season.

173 Average chloride concentration in May was $2.5 \pm 2.3 \text{ mg l}^{-1}$ (3 samples). Precipitation in June to September has relatively low
174 chloride concentrations, declining from $0.6 \pm 0.3 \text{ mg l}^{-1}$ to $0.26 \pm 0.12 \text{ mg l}^{-1}$ and $0.38 \pm 0.14 \text{ mg l}^{-1}$ at the end of the season.
175 Strong rain events in July and August have chloride concentrations between 0.2 and 0.3 mg l^{-1} . The annual wet chloride
176 deposition sums to $1.8 \pm 0.5 \text{ kg ha}^{-1}$. The measured values are in the range of published data (Goni et al., 2001; Laouali et al.,
177 2012; Bouchez et al. 2019; Gebru and Tesfahunegn, 2019). Dry deposition of chloride is estimated between 10 – 30% of wet
178 deposition (Bouchez et al. 2019).

179 **2.3 Soil and vegetation data**

180 At each study site, vertical soil profiles were core-drilled using a hand auger. In Salamat, soil profiles were sampled in 2016
181 (Tewolde et al., 2019) and 2019. In Waza Logone, soil samples were sampled in 2017 only (Tewolde et al., 2019), due to
182 security reasons in 2019. Each of the soil profiles was sampled in 10 cm intervals and filled into headspace glass vials and
183 plastic bags.

184 Each soil fraction was tested for grain size distribution using standard sieving and sedimentation procedures (Tewolde, 2017).
185 Classification follows the soil texture triangle by the US Department of Agriculture (Šimůnek et al., 2011).

186 Chloride concentration was analyzed after aqueous extraction from oven dried (105°C for 24 hours) soil samples following
187 the standard guideline DIN EN 12457-1 (Tewolde, 2017). Chloride concentrations in groundwater, which are used for
188 comparison, were measured using a DIONEX ICS-3000 ion chromatograph. Data are presented in Tables S2 and S3

189 Gravimetric water content is the mass of water contained in a sample as a percentage of the dried soil mass. It was obtained
190 by weighing the moist sample, oven drying it at 105°C for 24 to 48 hours, and weighing it again (Tables S2 and S3). Bulk
191 densities were not measured in the field, because of the difficulties handling the samples and sending them to the laboratory.
192 Instead, volumetric water contents were obtained by multiplying the gravimetric water contents for each soil type and location
193 by typical bulk densities obtained from the Global Gridded Surfaces of Selected Soil Characteristics database (Global Soil
194 Data Task Group, 2000), although accuracy of the calculated values reduces with sampling depth (Al-Shammmary et al., 2018).
195 The type of vegetation and the annual cycle of crops, length of the flooding period, and vegetation throughout the dry period
196 were mapped during field work and documented by surveying resident populations. In addition, MODIS vegetation indices
197 data (Didan, 2015) were used to justify the documented annual cycle of phenology (Figure 3).

198 3 Modelling methodology

199 Our approach assumes that groundwater recharge is controlled by precipitation, evaporation, and transpiration (surface runoff
200 can be neglected due to the flat topography). Soil moisture and chloride concentration along the soil profile at a certain time
201 are indicators for evaporation and transpiration processes within the root zone. Chloride concentration in soil depends on its
202 input via precipitation and washing out of dry deposition as well as on the amount of evaporation and transpiration on the soil
203 surface and in the root zone. We assume that amount of recharge corresponds to the volume of water that leaves the model
204 profile through the bottom boundary.

205 The first estimation of evapotranspiration was carried out using the FAO-dual crop coefficient approach that assesses E and T
206 individually. The uncertainty of E and T partitioning on soil water and chloride concentration in the six soil profiles was
207 assessed by considering scenarios of mean, maximum, and minimum E and T coefficients (see 3.1). Calculated time series of
208 E and T for the site-specific vegetation were used to estimate soil water and chloride concentration profiles at the sampling
209 time in each of the six locations using Hydrus-1D. A Bayesian approach was applied to consider uncertainties in chloride
210 concentrations of precipitation and dry deposition, in partitioning E and T as well as in the parametrisation of the soil hydraulic
211 model (Figure 4).

212 3.1 Partitioning of evaporation and transpiration

213 Evapotranspiration (ET) is the combination of two main processes driven by atmospheric demand: evaporation from the soil
214 (E) and transpiration through the stomata of plants (T) and is an important component of the water balance, especially in semi-
215 arid areas. The FAO provides a model (Allen et al., 1998) for estimating crop evaporation (ET_c) based on an empirically
216 defined crop coefficient (K_c) combined with a reference evapotranspiration (ET_0). Two approaches are possible, single crop
217 coefficient and dual crop coefficient. The latter was applied in this work.

218 The dual K_c method (Allen et al., 1998) is the sum of two coefficients, the basal crop coefficient (K_{cb}) that describes plant
219 transpiration and the soil water evaporation coefficient (K_e) that depicts evaporation from the soil surface. K_{cb} is defined as the
220 ratio of crop evapotranspiration over reference evapotranspiration (ET_c/ET_0), when the soil surface is dry and transpiration
221 occurs at a potential rate (i.e. unlimited water availability for transpiration). K_e is highest when the topsoil is wet, but diminishes
222 with drying out of topsoil to become zero, if no water remains near the soil surface for evaporation.

223 The parameters required for the estimation of monthly ET_c are the monthly reference evapotranspiration (ET_0), the monthly
224 basal crop coefficient (K_{cb}) and the monthly soil water evaporation coefficient (K_e):

$$225 \quad ET_c = ET_0 * K_c = ET_0 * (K_{cb} + K_e), \quad (2)$$

226 Onsite information on vegetation and phenology, such as month of planting, full emergence of crops, and harvesting times,
227 was used to define the monthly variation of vegetation at the study sites. These different vegetation periods were combined
228 with crop-specific K_{cb} values for sorghum and grass provided in Allen et al. (1998) for a sub-humid climate with relative
229 humidity of 45% and an average moderate wind speed of 2 m s^{-1} . To comply with the local semi-arid climate conditions in

230 Salamat and Waza Lagone, the coefficients K_{cb} for mid- and late-time vegetation periods were adjusted as proposed by Allen
231 et al. (1998). Monthly K_{cb} values for Acacia were estimated based on Do and Rocheteau (2003) and Do et al. (2008). Site-
232 specific monthly variation of ground cover and flooding periods with ranges of crop coefficient (K_{cb}), soil water evaporation
233 coefficient (K_e), and root depth are provided in Table S4.

234 **3.2 Modelling water flow and solute transport**

235 **3.2.1 Model concept, setup, and initial conditions**

236 The chloride profiles measured in soil at a certain time represent water and solute budget input from past precipitation events
237 and can be estimated by transient water flow and solute transport modelling. The model concept assumes that atmospheric
238 chloride input is restricted to solute in precipitation and that the chloride concentration profile results from solute enrichment
239 in the soil, due to evaporation and transpiration. An accurate parametrization of the unsaturated flow and transport model as
240 well as a robust quantification of groundwater recharge are not possible with the available data and hence cannot be included
241 within the scope of this study. However, the model results estimate groundwater recharge magnitude and variability based on
242 information regarding soil texture and vegetation as well as associated uncertainty in results. This proposed approach is
243 appropriate for locations with limited availability of long-term soil water measurements.

244 The free software package Hydrus-1D version 4.17.0140 was used to simulate transient water flow and solute transport in the
245 six variably saturated soil profiles. Hydrus-1D numerically solves the Richards (1931) equation for variably saturated water
246 flow, advection-dispersion equations for heat, and solute transport (Šimůnek et. al, 2009):

$$247 \frac{\partial \theta(h)}{\partial t} = \frac{\partial}{\partial z} \left[K(h) \left(\frac{\partial h}{\partial z} + \cos \alpha \right) \right] - S(h) \quad (3)$$

248 with:

- 249 h soil water pressure head [L]
250 θ volumetric water content [L^3L^{-3}]
251 t time [T]
252 z spatial coordinate [L] (positive upwards)
253 S sink term [$L^3L^{-3}L^{-1}$]
254 α angle between flow direction and vertical axis
255 $K(h)$ unsaturated hydraulic conductivity function [LT^{-1}]

256

257 The processes simulated at the six study sites were water flow, solute transport, and root water uptake. Hydrus-1D requires
258 input data at daily time steps, but available precipitation and evaporation data were monthly. Daily values were calculated
259 dividing monthly data by month-specific days. Thus, all days in a month had the same precipitation rate and the same
260 evapotranspiration rate. Model execution ended at the soil sampling time (December 2016 and July 2019 for Salamat and June
261 2017 for Waza Logone). Progressive root growth was considered in all profiles except for ST2, in which the roots of the Acacia

262 trees were distributed along the whole profile and assumed invariant over the simulation period. Since initial conditions of soil
 263 moisture and resident chloride concentration are unknown, arbitrary values were adopted. To account for different residence
 264 times of water and chloride, due to different degrees of evapotranspiration and unknown initial conditions, each model was
 265 run over a period of time long enough to allow the exchange of at least one water column volume. Thus, total modelling periods
 266 are different depending on the soil type at each site: ST1, ST2 start in 1910, which leads to a maximum residence time (MRT)
 267 of 106 years; ST3 in 2010 (MRT = 6 years), WL1 and WL2 in 1990 (MRT = 26 years), and WL3 in 1970 (MRT = 46 years).
 268 All profiles were discretized into 101 nodes and different horizons according to the soil types interpreted from the individual
 269 grain size distributions.

270 3.2.2 Water flow

271 For calculation of water retention (θ) and unsaturated hydraulic conductivity functions ($K(h)$), the Mualem-van Genuchten
 272 (MVG) model (van Genuchten, 1980) was applied:

$$273 \theta(h) = \begin{cases} \theta_r + \frac{\theta_s - \theta_r}{[1 + |\alpha h|^n]^m} & h < 0 \\ \theta_s & h \geq 0 \end{cases} \quad (4)$$

274

$$275 k(h) = k_s S_e^{-1} \left[1 - (1 - S_e^{l/m})^m \right] \quad (5)$$

276 where:

$$277 m = 1 - \frac{1}{n}; \quad n > 1$$

$$278 S_e = \frac{\theta(h) - \theta_r}{\theta_s - \theta_r}$$

279 with

280 θ water content [$L^3 L^{-3}$]

281 h hydraulic head [L]

282 θ_r residual water content

283 θ_s saturated water content

284 α inverse of the air-entry value, empirical [L^{-1}]

285 n pore-size distribution index, empirical [-]

286 l pore-connectivity parameter, empirical ≈ 0.5 [-]

287 S_e effective saturation [-]

288 k_s saturated hydraulic conductivity [LT^{-1}]

289

290 To reduce computational effort, the initial parametrization of these functions was realized using pedotransfer functions
291 implemented in Rosetta (Schaap et al., 2001), which is a dynamically-linked library coupled to Hydrus-1D. The input
292 parameters for each profile were the percentages of sand, silt, clay, and bulk density at several depths. Whenever consecutive
293 layers of a profile showed almost the same grain size distribution (texture) and soil moisture, the layers were lumped together
294 and parameter averages were used in the model. The tortuosity parameter l [-] of the MVG was set to 0.5 as proposed by
295 Mualem (1976).

296 The upper boundary condition was defined as a variable atmospheric condition, whereas the lower boundary was set to zero-
297 gradient with free drainage of water for all profiles, except WL3 where confined groundwater conditions prevailed below the
298 confining clay layer encountered at 3.9 m depth. During drilling, groundwater was hit at 3.9 m depth, but rapidly rose to 2.6 m
299 below surface. Consequently, a constant head condition was implemented at 2.6 m depth.

300 **3.2.3 Root water uptake and root growth**

301 The sink term (S) in the Richards' equation, defined by Feddes et al. (1978) as the volume of water removed from a unit
302 volume of soil per unit time due to plant water uptake, was considered in all soil profiles according to the prevailing vegetation
303 (Table S4). The Feddes' default parameters for grass were used in the ST3 and Waza Logone profiles. In ST1, where sorghum
304 was planted, Feddes' parameters for corn were used because sorghum is not available in the list. According to Righes (1980)
305 sorghum and corn roots extract water from approximately the same soil depths and have similar average root density
306 distribution.

307 An average root depth of 1 m was adopted in ST1 for the initial and end seasons, and 2 m for development and mid seasons.
308 In the case of Acacia in ST2, the adopted parameters correspond to deciduous trees. The root depth of the Acacia tree was
309 considered as constant over the entire simulation period with maximum root distribution at 0.5 m and decreasing distribution
310 down to 2 m (Beyer et al., 2016). In ST3, the vegetation was defined as grass, while in WL1, WL2 and WL3 it was defined as
311 grass with a flooding period of 3 months in WL1 and WL3, but only one month in WL2. Rooting depth values used at these
312 sites range from 0.1 m to 0.5 m, depending on the growth stage of grass. The median maximum rooting depth value of annual
313 grass in water-limited ecosystems is 0.37 m with a 95% confidence level in an interval of 0.26 m-0.55 m (Schenk and Jackson,
314 2002).

315 **3.2.4 Solute transport**

316 The chloride concentration in soil water was simulated using an equilibrium advection-dispersion model implemented in
317 Hydrus1D. Hydrodynamic dispersion was implemented considering dispersivity values of 1/10th of the individual layer
318 thickness, a molecular diffusion coefficient of $1.3 \times 10^{-9} \text{ m}^2\text{s}^{-1}$, and a tortuosity factor as defined by Millington and Quirk
319 (1961). Adopted dispersivity values are within reported ranges of 0.08 m to 0.20 m (Vanderborcht and Vereecken, 2007;
320 Stumpp et al, 2009, 2012).

321 A time-dependent concentration boundary condition was applied to the upper boundary and a zero-gradient boundary condition
322 to the lower boundary. The transient liquid phase concentration of infiltrating rainwater follows measured chloride
323 concentration in precipitation sampled in N'Djamena. The chloride concentration of ponding water correspond to four values
324 measured in Salamat that range from 2.5 mg l⁻¹ to 25 mg l⁻¹ with an average of 9 mg l⁻¹. Initial chloride concentration in soil
325 water was set to 0 mg l⁻¹. However, each model was run over a period of time long enough to allow the exchange of at least
326 one water column volume (3.2.1). The model does not consider root solute uptake.

327 **3.2.5 Crop evapotranspiration scenario definition**

328 Since crop evapotranspiration was not measured, values were simulated using K_{cb} , K_e , and root depth instead. Because these
329 parameters are given in ranges (Table S4), seven scenarios with different combinations of K_{cb} , K_e , and root depth were
330 developed to assess ranges of crop evaporation (Table 2). Scenario “Mean” corresponds to the average value of all parameters.
331 Scenarios “Min” and “Max” combine the minimum and maximum values, respectively. Scenario “Mix-1” combines minimum
332 K_{cb} with average K_e and root depth, scenario “Mix-2” minimum K_e with average K_{cb} and root depth whereas scenario “Mix-
333 3” combines minimum root depth with average K_e and K_{cb} .

334 **3.2.6 Bayesian model calibration**

335 Based on the crop evapotranspiration scenarios, the models were calibrated and model uncertainty was estimated using a
336 Bayesian calibration. Bayesian analysis is a combination of the data likelihood and the prior distribution using the Bayes
337 theorem (ter Braak and Vrugt, 2008). The sum of likelihood functions for soil moisture and chloride concentration was
338 implemented to calculate the log-likelihood of a simulation given the observations and standard deviations at each calibration
339 step. The posteriori parameter distribution was estimated using the Differential Evolution Markov Chain Monte-Carlo (DE-
340 MCzs) algorithm with three sub-chains (ter Braak and Vrugt, 2008) implemented in the R package BayesianTools (Hartig et
341 al., 2019). The number of iterations was defined individually according to a Gelman-Rubin reduction factor < 1.2.

342 In the calibration, scaling factors ranging from 0.75 to 1.25 for the MVG parameters (saturated volumetric water content,
343 alpha, and n) were adopted individually. However, ranges for the MVG model parameter n were constrained to $n > 1.01$. Log-
344 transformed saturated hydraulic conductivity for each layer was considered with ranges from -0.5 to 0.5. The scaling factor
345 for transpiration was simultaneously used as a divisor for evaporation to remain within the calculated rate of ET_0 . From all
346 accepted model runs, 100 were randomly selected at each individual location to evaluate average model results and standard
347 deviations.

348 4 Results

349 4.1 Grain size distribution

350 Soil textures were defined based on grain size distributions of the six profiles (Figure 5) according to the US Department of
351 Agriculture soil texture triangle. Most profiles are fine-grained soils (clay, sandy clay) and fine-grained soils with intercalation
352 of thin sand and loam layers. Only soil profile ST3 is dominated by sand and sandy clay loam.

353 4.2 Model parametrization

354 The calibrated parametrization of the MVG model for each layer of the six sampling locations is plausible (Table 3). The
355 posterior distributions of the Bayesian calibration show the sensitive parameters of the model fit. For ST1, these are n , θ_s ,
356 chloride concentration, and the transpiration fraction in evapotranspiration (T), but the k_s is less sensitive (Fig. S1). For ST2,
357 the sensitivities of the model parameters are similar with k_s of the upper layer being the most sensitive and chloride
358 concentration the least sensitive (Fig. S2). The model fits of the data from site ST3 are generally insensitive. Only α , n , and k_s
359 of the upper layer as well as chloride concentration show tighter posteriori distributions (Fig. S3). For site WL1, the model
360 parameters n of layers 1, 2, and 3 as well as the saturated water content of layers 3 and 5, and subordinately of layer 4, are
361 sensitive (Fig. S4). For WL2, the model parameters n of all layers, k_s of layer 3, and θ_s of layers 2 and 3 are sensitive (Fig. S5).
362 For WL3, θ_s of layer 2, k_s of layers 1 and 2, and the fraction of transpiration in evapotranspiration are sensitive (Fig. S6).

363 4.3 Soil water content, chloride concentration and groundwater recharge

364 Measured and simulated water content and chloride concentration profiles for individual scenarios are shown in Figure 6. The
365 average root mean squared error (RMSE) of simulated water content for all individual scenarios ranges from 0.02 to 0.06 cm^3
366 cm^{-3} (Table 4). In general, the models reproduce well the water content and chloride concentrations. However, the dynamics
367 of measured and simulated water contents differ considerably for ST1 and partly for ST2, although maximum values do match.
368 This is due to the long chloride residence time in both locations (109 years) in comparison to the length of data availability (49
369 years for precipitation and 6 years for chloride concentrations). The models do not match the high chloride concentrations in
370 the uppermost part of soil profiles for ST3, WL1, and WL2. The standard deviations in chloride concentration of the randomly
371 selected model runs are exceptionally high in the lower part of ST2 that corresponds to the poor sensitivity of the chloride
372 concentration at the upper boundary and the comparably wide range of measured chloride concentration in ponding water in
373 the Salamat region ($2.5 \text{ mg l}^{-1} - 25 \text{ mg l}^{-1}$).

374 Measured chloride concentrations in groundwater are much lower compared to those in soil profiles (Tables S2 and S3). This
375 is because groundwater encountered in the study area has been recharged in regions, where chloride input does not play an
376 important role. Large amounts of recharge for the Quaternary aquifer occur mainly in the southern part of the Lake Chad Basin,
377 where long-term annual precipitation reaches values over 1000 mm. Any chloride accumulated in the soil is well diluted and
378 washed away periodically.

379 However, the large differences in chloride concentrations between soils and groundwater demonstrate the enormous
380 accumulation capacity of soils in the Lake Chad Basin, which act as a buffer over years until precipitation is high enough to
381 dilute the profile. This effect is depicted by the different chloride concentrations measured in profile ST1 between 2016 and
382 2019 (Table S2) and by the model results for profile ST2 (Figure 7).

383 The interannual variability of modelled groundwater recharge differs considerably among locations (Figure 7, Table 5). In
384 general, interannual groundwater recharge variability depends on vegetation and soil texture with related water retention
385 capacity. Vegetation with deep roots on soil with comparably high water retention capacity have a stronger interannual
386 variability, e.g. at ST1, ST2 where recharge occurs only in years with high precipitation. Fine textured soils with shallow
387 rooting vegetation have an intermediate variability (WL1, WL2, and WL3), where years without recharge occur only during
388 drought periods. The coarser textured soils with grass cover have low interannual recharge variability (ST3) and recharge
389 occurs each year. Years with high precipitation, e.g. 2006, 2007, and 2008 in Waza Logone as well as 2010 in Salamat,
390 produced strong groundwater recharge.

391 The highest average annual recharge (93 mm) was calculated for ST3 in Salamat (Table 6), where the water balance during
392 the rainy season (July-September) is higher compared to the Waza Logone region, and where shallow rooting vegetation
393 prevails on comparably coarse soil texture with low water retention capacity and higher hydraulic conductivity. The other
394 locations in Salamat have lower calculated annual recharge, due to deep rooting vegetation and higher soil water retention
395 capacity. The impact of soil texture on annual groundwater recharge becomes apparent by comparing the three locations in
396 Waza Logone with the same vegetation on soils with different water retention capacities and hydraulic conductivities.
397 Groundwater recharge expressed as a fraction of precipitation is between 1% and 4% (Table 5), which is within the range of
398 0.1 to 5% published by Scanlon et al. (2006). Only at WL2 (8%) and ST3 (12%), where coarse soil textures enhance recharge,
399 a comparably high fraction is estimated.

400 Simulated chloride concentration and water budget of the soils over the simulated time-period are rather unstable and differ
401 for the six locations. At location ST2 with clay loam soil covered by Acacia and grass, accumulation of chloride takes place
402 over several years, due to the high transpiration related to the effective field capacity. However, in high precipitation years,
403 most of the accumulated chloride is leached to groundwater and soil concentration diminishes, which can be seen from the
404 time-varying differences of the cumulative solute fluxes between the top and bottom boundaries (Figure 8). The difference of
405 cumulative solute flux at the top and bottom boundaries represents the magnitude of chloride accumulation in soil. It should
406 be noted that at this site, the measured chloride concentrations cannot be reconstructed, if only input via precipitation is
407 considered. The measured profile can only be plausibly modelled with an additional input via ponding water. Chloride input
408 at the upper boundary is consequently six-times higher at ST2 compared to the other locations considered in this study.

409 At location ST3, the chloride accumulation is much lower compared to the other locations. The chloride budget is controlled
410 by the fast groundwater recharge response to precipitation, which flushes chloride annually from the soil towards the
411 groundwater. Most of the chloride that infiltrated with precipitation remains in the vadose zone over several years and is

412 leached towards groundwater mainly during years with precipitation or water infiltration above threshold values (Figure 8).
413 Chloride accumulation is highest in profiles with clay soils and high effective field capacity (ST1, WL1, and WL3).
414 Chemical memory effects are subject to the dynamics of the water and chloride balance. Therefore, steady-state assumptions
415 are unsuitable. Accurate estimations are only possible with transient assumptions.

416 **4.4 Evaporation and transpiration**

417 The amount of transpiration depends on the availability of water in the root zone and the type of vegetation cover. At ST1,
418 annual transpiration presents two peaks: one related to sorghum and the other to grass (Figure 9). At each location and in every
419 simulation year, soil water content in the root zone reaches the wilting point defined by the specific parametrization of the root
420 water uptake model.

421 The actual evaporation rate depends mainly on the availability of water in the upper soil zone (Table 6), but calculated values
422 are in accordance with other studies in the area (Bouchez et al., 2019). Clay and clay-loam with relatively high water storativity
423 have larger amounts of evaporated water compared to sand and loam soils. During dry seasons, the uppermost part of the soils
424 dries up annually, which significantly restricts evaporation.

425 Actual evapotranspiration is lower than the reference evapotranspiration most of the year. During and shortly after the rainy
426 season, when sufficient soil water is available, actual evapotranspiration is comparable to or higher than ET_0 depending on the
427 vegetation.

428 **5 Discussion**

429 Soil texture information is helpful to constrain the MVG parameter ranges while searching for realistic parameter sets
430 (Sprenger et al., 2015). However, poor representation of soil moisture dynamics using MVG parameters derived using Rosetta
431 are reported (Sprenger et al., 2015) suggesting that soil structure has to be taken into account (Vereecken et al., 2010),
432 especially for soils where high rock content influences water flow due to inherent heterogeneity (Sprenger et al., 2015). The
433 soils at the locations considered in this study belong to Quaternary sediments in the Lake Chad basin and heterogeneity due to
434 rock fragments is largely absent. Furthermore, soil moisture dynamics over the year are much higher in soils of the Waza
435 Logone floodplain compared to soils from the more humid regions in the south, where annual precipitation, although high,
436 occurs only over 4-5 months. It is expected that high soil moisture dynamics, rather homogeneous soils, and the monthly
437 resolution of climate data result in a minor impact of soil structure on MVG parametrization and groundwater recharge as
438 shown in Section 3.2. Soil moisture dynamics at all locations considered in this study are limited by water availability for
439 evaporation in the uppermost part of the soil and by water uptake in the root zone, but not by the reference evapotranspiration.
440 However, because time resolution of precipitation and evapotranspiration data is monthly, the models probably underestimate
441 soil moisture dynamics.

442 Calculated chloride concentrations for the soil profiles give indications of appropriate MVG parametrization as well as
443 evaporation and transpiration partitioning. However, uncertainty of chloride input and its transient variability in particular is

444 expressed in rather wide and partly bimodal distributions of the scaling factor (sc_Conc) included in the calibration (Figures
445 S1-S6 in supplement material). On one hand, measured chloride concentrations in precipitation are in agreement with other
446 studies in central Africa (Goni et al., 2001; Laouali et al., 2012; Gebru and Tesfahunegn, 2019) and its transient behaviour
447 within the rainy season is considered in the applied model. On the other hand, impact of dry deposition is unknown, because
448 of data scarcity and potential lateral flow of periodic flooding. Furthermore, due to the monthly resolution of the atmospheric
449 boundary condition, extreme rain events that cause surface runoff cannot be reflected in the model. The variability of chloride
450 concentration in some of the soil profiles, which cannot be completely reproduced by the model, indicates either a higher
451 variability of chloride input and/or a larger variability in soil physics.

452 Bouchez et al. (2019) identified a chloride deficit between deposition and river export in the Chari-Logone river system of
453 88% (only 12% of the deposited chloride is exported via river water). They refer to the chemical memory effect, which can
454 play an important role in arid regions. Our simulations show the importance of the vadose zone for storage of chloride over
455 longer periods of time, which explains the fate of chloride in the basin and confirms the chemical memory effect. In this
456 context, it must be noted that the thickness of the vadose zone at the locations considered in this study is between 4 m and
457 21 m, where important amounts of chloride can be potentially stored leading to a strong delay of the chemical signal from
458 precipitation to groundwater.

459 Time-dependent recharge cannot be verified with groundwater hydrographs, because these data are not available in the study
460 area. However, the calculated mean annual groundwater recharge values are within the ranges of 0.2 to 35 mm yr⁻¹ estimated
461 by Edmunds et al. (2002) using the CMB method in seven chloride profiles in northern Nigeria. The larger values (90 mm yr⁻¹
462 in ST3 and 54 mm yr⁻¹ in WL2) are due to local coarse soil and fall within the values estimated by Bouchez et al. (2019),
463 who, based on ³⁶Cl and Cl budgets in groundwater, propose recharge values between 16 mm yr⁻¹ and 240 mm yr⁻¹.

464 **6 Conclusions**

465 The quantitative estimation of groundwater recharge in the LCB is difficult due to the scarce data availability and the expected
466 low recharge quantities. Estimation of low recharge amounts in arid and semi-arid areas are usually ambiguous, because the
467 inherent measurement inaccuracies lead to uncertainties during data processing and modelling. Quantification of water and
468 solute fluxes in the vadose zone is often implemented using long-term time series of soil moisture, pressure heads, and
469 concentration data in combination with appropriate models. Monitoring of soil moisture and solute concentration over longer
470 periods at different depths and sites is difficult in the LCB, due to limited infrastructure and challenging climatic boundary
471 conditions. The presented approach combines soil moisture and chloride concentration quantified along vertical soil profiles
472 in different locations within the LCB with numerical models and freely accessible data, while considering data uncertainty.
473 Calculated chloride concentrations for the soil profiles provide appropriate MVG parametrization as well as evaporation and
474 transpiration partitioning. Although measured and simulated dynamic behaviour of both water contents and chloride
475 concentrations differ considerably in profiles ST1 and partly in ST2, their magnitudes largely agree. This is especially
476 important for chloride concentrations in the middle and deeper parts of the profiles, where seasonal effects are mainly averaged.

477 Thus, the estimates of soil water balance and especially of groundwater recharge as well as the adopted soil physical parameters
478 are plausible.

479 Mean groundwater recharge values estimated in this study are different from those published in Tewolde et al. (2019). This is
480 due to the more extensive availability of chloride concentration data in precipitation for this study. In addition, Tewolde et al.
481 (2019) roughly estimated one value of saturated porosity for each profile. This parameter is rather sensitive in the Bayesian
482 calibration and several values along each of the profiles were considered in this study. In contrast to the assessment of
483 groundwater recharge with the CMB (Tewolde et al., 2019), the method used here allows not only estimates of mean recharge,
484 but also its interannual dynamics, variability, and the classification of the uncertainties of the input data and modelling results.
485 The interannual variability of groundwater recharge is generally higher than the uncertainty of the modelled groundwater
486 recharge. The soil moisture dynamics at all locations considered in this study are limited by water availability for evaporation
487 in the uppermost part of the soil and by water uptake in the root zone and not by the reference evapotranspiration.
488 Simulations show the importance of the vadose zone for storage of chloride over longer time-periods and explain the fate of
489 chloride in the basin. The thickness of the vadose zone at the locations considered in this study varies between 4 m and 21 m.
490 Important amounts of chloride can be potentially stored significantly delaying the chemical signal from precipitation to
491 groundwater.
492 Upscaling of the results to larger areas must be interpreted with caution since the considered combinations of soils and
493 vegetation probably do not cover all combinations present in the Salamat and Waza Logone regions.

494 **Author contribution**

495 M.R. conducted fieldwork; A.G.M.S. and C.N. conducted modelling and interpretation; C.N. and S.V. designed the study and
496 completed the writing. All authors contributed to the discussion of results and commented on the manuscript.

497 **Acknowledgement**

498 This study was conducted within the framework of the technical cooperation project “Lake Chad Basin - Management of
499 Groundwater Resources” jointly executed by the Lake Chad Basin Commission (LCBC) and the German Federal Institute for
500 Geosciences and Natural Resources (BGR). The technical project is funded by the German Federal Ministry for Economic
501 Cooperation and Development (BMZ). We thank Daniel Tewolde, Paul Königer and Anna Degtjarev for their support in the
502 lab. We are highly indebted to John Molson for the thorough linguistic review of our manuscript.

503 **References**

504 Allen, R. G., Pereira, L. S., Dirks, R., Smith, M.: Crop evapotranspiration: Guidelines for computing crop water requirements.
505 FAO Irrigation and Drainage Paper No. 56. Rome, Italy. <https://doi.org/10.1016/j.eja.2010.12.001>, 1998.
506 Al-Shammary, A. A. G., Zouzani, A. Z., Kaynak, A., Khoo, A. Y., Norton, M., Gates, W.: Soil bulk estimation methods: A
507 review. *Pedosphere*, 28(4), 581-596. [https://doi.org/10.1016/S1002-0160\(18\)60034-7](https://doi.org/10.1016/S1002-0160(18)60034-7), 2018.

508 Alves, M. E. B., Mantovani, E. C., Sediya, G. C., Neves, J. C. L.: Estimate of the crop coefficient for Eucalyptus cultivated
509 under irrigation during initial growth. *Cerne*, 19(2), 247–253. <https://doi.org/10.1590/s0104-77602013000200008>, 2013

510 Anderson, R. G., Zhang, X., Skaggs, T. H.: Measurement and Partitioning of Evapotranspiration for Application to Vadose
511 Zone Studies. *Vadose Zone Journal*, 16(13), 0. <https://doi.org/10.2136/vzj2017.08.0155>, 2017

512 Aouade, G., Ezzahar, J., Amenzou, N., Er-Raki, S., Benkaddour, A., Khabba, S., Jarlan, L.: Combining stable isotopes, Eddy
513 Covariance system and meteorological measurements for partitioning evapotranspiration, of winter wheat, into soil
514 evaporation and plant transpiration in a semi-arid region. *Agricultural Water Management*, 177, 181–192.
515 <https://doi.org/10.1016/J.AGWAT.2016.07.021>, 2016.

516 Bader, J., Lemoalle, J., Leblanc, M.: Modèle hydrologique du Lac Tchad, *Hydrolog. Sci. J.*, 56, 411–425, 2011.

517 Batello, C., Marzot, M., Harouna Touré, A.: The future is an ancient lake: Traditional knowledge, biodiversity and genetic
518 resources for food and agriculture in the Lake Chad basin ecosystems. FAO Interdepartmental Working Group on Biological
519 Diversity for Food and Agriculture, Rome, 2004.

520 Bernacsek, G. M., Hughes, J. S., Hughes, R. H. (Ed.): A directory of African wetlands. International Union for the
521 Conservation of Nature and Natural Resources, 1992.

522 Beyer, M., Koeniger, P., Himmelsbach, T.: Constraining water uptake depths in semi-arid environments using stable water
523 isotopes Results & Discussion. <https://doi.org/10.5281/zenodo.56159>, 2016.

524 Boronina, A., Favreau, G., Coudrain, A., Dieulin, C., Zairi, R.: Data scarcity in the large semiarid Lake Chad basin:
525 incorporating environmental tracers as a priori information for groundwater modelling. ModelCare 2005, Scheveningen, The
526 Netherlands, 2005.

527 Bouchez, C., Goncalves, J., Deschamps, P., Vallet-Coulomb, C., Hamelin, B., Doumnang, J.C., Sylvestre, F.: Hydrological,
528 chemical, and isotopic budgets of Lake Chad: a quantitative assessment of evaporation, transpiration and infiltration fluxes,
529 *Hydrol. Earth Syst. Sci.*, 20, 1599–1619, 2016.

530 Bouchez, C., Deschamps, P., Goncalves, J., Hamelin, B., Nour, A.M., Vallet-Coulomb, C., Sylvestre, F.: Water transit time
531 and active recharge in the Sahel inferred by bomb-produced ³⁶Cl. *Nature, scientific reports*, 9: 7465, 2019.

532 Carmouze, J.-P.: Originalité de la régulation saline du lac Tchad, *Comptes Rendus de l'Académie des Sciences. Série D:*
533 *Sciences Naturelles*, 275, 1871–1874, 1972.

534 Cuthbert, M. O., Taylor, R.G., Favreau, G. et al.: Observed controls on resilience of groundwater to climate variability in sub-
535 Saharan Africa. *Nature*, 572: 230-234. <https://doi.org/10.1038/s41586-019-1441-7>, 2019.

536 Didan, K.: MOD13Q1 MODIS/Terra Vegetation Indices 16-Day L3 Global 250m SIN Grid V006. NASA EOSDIS Land
537 Processes DAAC. <https://doi.org/10.5067/MODIS/MOD13Q1.006>, 2015.

538 Didane, D. H., Rosly, N., Zulkafli, M. F., Shamsudin, S. S.: Evaluation of wind energy potential as a power generation source
539 in Chad. *International Journal of Rotating Machinery*, vol. 2017, Article ID 3121875, 10 pp, 2017.

540 Do, F., Rocheteau, A.: Cycle annuel de transpiration d'Acacia raddiana par la mesure des flux de sève brute (Nord-Sénégal).
541 In *Un arbre au désert: Acacia raddiana* (pp. 119–142). Paris, 2003.

542 Do, F., Rocheteau, A., Diagne, A. L., Goudiaby, V., Granier, A., Lhomme, J. P.: Stable annual pattern of water use by *Acacia*
543 *tortilis* in Sahelian Africa. *Tree Physiology*, 28(1), 95–104. <https://doi.org/10.1093/treephys/28.1.95>, 2008.

544 Eberschweiler, Ch.: Suivi et gestion des ressources en eaux souterraines dans le bassin du lac Tchad – Prémодélisation des
545 systèmes aquifères, évaluation des ressources et simulation d’exploitation. Rapport. BRGM/CBLT.

546 Edmunds, W. M., Gaye, C.B.: Estimating the spatial variability of groundwater recharge in the Sahel using chloride. *J. Hydrol.*,
547 156(1-4):47-59, 1994.

548 Edmunds, W. M., Fellman, E., Goni, I. B.: Spatial and temporal distribution of groundwater recharge in northern Nigeria.
549 *Hydrogeology Journal*, 10:205-215, 2002.

550 Feddes, R. A., Kowalik, P. J., Zaradny, H.: Simulation of field water use and crop yield. Published in 1978 in Wageningen by
551 Centre for agricultural publishing and documentation. Wageningen: Centre for Agricultural Pub. and Documentation.
552 <https://lib.ugent.be/catalog/rug01:000032129>, 1978.

553 Fontes, J.-C., Maglione, G., Roche, M.-A.: Données isotopiques préliminaires sur les rapports du lac Tchad avec les nappes
554 de la bordure nord-est, *Cah. Orstom. Hydrobiol.*, 6, 17– 34, 1969.

555 Fontes, J.-C., Gonfiantini, R., Roche, M.-A. : Deuterium et oxygène-18 dans les eaux du Lac Tchad. *Isotope Hydrology*, IAEA-
556 SM-129/23, 1970.

557 Gebru, T.A., Tesfahunegn, G.B.: Chloride mass balance for estimation of groundwater recharge in a semi-arid catchment of
558 northern Ethiopia. *Hydrogeology Journal*, 27:363-378, 2019.

559 Global Soil Data Task Group: Global Gridded Surfaces of Selected Soil Characteristics (IGBP-DIS). ORNL DAAC, Oak
560 Ridge, Tennessee, USA. <https://doi.org/10.3334/ORNLDAAC/569>, 2000.

561 Goni, I., Fellman, E., Edmunds, W.: Rainfall geochemistry in the Sahel region of northern Nigeria, *Atmos. Environ.*, 35, 4331–
562 4339, 2001.

563 Goni, I., Taylor, R., Favreau, G., Shamsudduha, M., Nazoumou, Y., Ngouno Ngatcha, B.: Groundwater recharge from heavy
564 rainfall in the southwestern Lake Chad Basin: evidence from isotopic observations. *Hydrological Sciences Journal*.
565 <https://doi.org/10.1080/02626667.2021.1937630>, 2021.

566 Groh, J., Stumpp, C., Lücke, A., Pütz, T., Vanderborght, J., Vereecken, H.: Inverse estimation of soil hydraulic and transport
567 parameters of layered soils from water stable isotopes and lysimeter data, *Vadose Zone Journal* 17:170168.
568 <https://doi.org/10.2136/vzj2017.09.0168>, 2018.

569 Gröning, M., Lutz, H.O., Roller-Lutz, Z., Kralik, M., Gourcy, L., Pölsenstein, L.: A simple rain collector preventing water re-
570 evaporation dedicated for $\delta^{18}\text{O}$ and $\delta^2\text{H}$ analysis of cumulative precipitation samples. *J. Hydrol.* 448-449, 195-200, 2012.

571 Harris, I., Osborn, T. J., Jones, P., Lister, D.: Version 4 of the CRU TS monthly high-resolution gridded multivariate climate
572 dataset. *Sci. Data* 7, 109. <https://doi.org/10.1038/s41597-020-0453-3>, 2020.

573 Isihoro, S., Matisoff, G., Wehn, K.: Seepage relationship between Lake Chad and the Chad Aquifers, *Groundwater*, 34, 819–
574 826, 1996.

575 Hartig, F., Minunno, F., Paul, S.: BayesianTools: General-Purpose MCMC and SMC Samplers and Tools for Bayesian
576 Statistics, 2019.

577 Jasechko, S., Sharp, Z. D., Gibson, J. J., Birks, S. J., Yi, Y., Fawcett, P. J.: Terrestrial water fluxes dominated by transpiration,
578 Nature, 496, 347–350, 2013.

579 Kool, D., Agam, N., Lazarovitch, N., Heitman, J. L., Sauer, T. J., Ben-Gal, A.: A review of approaches for evapotranspiration
580 partitioning. Agricultural and Forest Meteorology, 184, 56–70, 2014.

581 Lake Chad Basin Commission: Monitoring and management of groundwater resources in the Lake Chad Basin. Mapping of
582 aquifers, water resources management, final report, R35985, Report BRGM R 35985 EA U/4S/93, 1993.

583 Lake Chad Basin Commission: Report on the State of the Lake Chad Basin Ecosystem.
584 http://www.cbtl.org/sites/default/files/download_documents/report_on_the_state_of_the_lake_chad_basin_ecosystem.pdf,
585 2012.

586 Laouali, D., Galy-Lacaux, C., Diop, B., Delon, C., Orange, D., Lacaux, J.P., Akpo, A., Lavenu, F., Gardrat, E., Castera, P.:
587 Long term monitoring of the chemical composition of precipitation and wet deposition fluxes over three Sahelian savannas.
588 Atmos. Environ. 50, 314–327. <https://doi.org/10.1016/j.atmosenv.2011.12.004>, 2012.

589 Leblanc, M.: Gestion des ressources en eau des grands bassins semi-arides à l'aide de la télédétection et des SIG: application
590 à l'étude du bassin du lac Tchad, Afrique, PhD thesis, Université de Poitiers, Poitiers, 2002.

591 Leblanc, M.: The Use of Remote Sensing and GIS for Water Resources Management of Large Semi-Arid Regions : a Case
592 Study of the Lake Chad Basin, Africa. PhD Thesis, University of Glamorgan and University of Poitiers, 2002.

593 Leblanc, M., Favreau, G., Tweed, S., Leduc, C., Razack, M., Mofor, I.: Remote sensing for groundwater modelling in large
594 semiarid areas: Lake Chad basin, Africa. Hydrogeology Journal, 15(1), 97-100, 2007.

595 Lemoalle, J., Bader, J.-C., Leblanc, M., Sedick, A.: Recent changes in Lake Chad: observations, simulations and management
596 options (1973–2011), Global Planet. Change, 80, 247–254, 2012.

597 Lemoalle, J., Magrin, G.: Le développement du lac Tchad: situation actuelle et futurs possibles. Marseille, IRD Éditions, coll.
598 Expertise collégiale, bilingue français-anglais, 216 p., 2014.

599 Lloyd, J. W.: A review of aridity and groundwater, Hydrological Processes, Vol. 1, 63-78, 1986.

600 Lloyd, J. W.: Groundwater in arid and semiarid regions. In: Silveira, L. and Usunoff E.J. [Eds.]: Groundwater (Vol. I),
601 Encyclopedia of Life Support Systems, pp. 284–307, 2009.

602 Majnooni-Heris, A., Sadraddini, A. A., Nazemi, A. H., Shakiba, M. R., Neyshaburi, M. R., Tuzel, I. H.: Determination of
603 single and dual crop coefficients and ratio of transpiration to evapotranspiration for canola. Annals of Biological Research,
604 3(4), 1885–1894, 2012.

605 Massuel, S.: Modélisation hydrodynamique de la nappe phréatique quaternaire du bassin du lac Tchad. Diplôme d'études
606 approfondies, Université de Montpellier II, Université d'Avignon et des pays du Vaucluse, 2001.

607 Mertens, J., Barkle, G. F., Stenger, R.: Numerical analysis to investigate the effects of the design and installation of equilibrium
608 tension plate lysimeters on leachate volume, Vadose Zone Journal, 4:488-499, 2005.

609 Millington, R. J., Quirk, J. P.: Permeability of porous solids. *Trans. Int. Congr. Soil Sci.*, 7(1), 97-106, 1961.

610 Mualem, Y.: A new model for predicting the hydraulic conductivity of unsaturated porous media, *Water Resour. Res.*, 12,
611 513–522. <https://doi.org/10.1029/WR012i003p00513>, 1976.

612 Ngatcha, B. N., Mudry, J., Leduc, C.: The state of understanding on groundwater recharge for the sustainable management of
613 transboundary aquifer in the Lake Chad basin, 2008.

614 Olivry, J., Chouret, A., Vuillaume, G., Lemoalle, J., Bricquet, J.: *Hydrologie du lac Tchad*, Editions de l'ORSTOM, Paris
615 1996.

616 Richards, L. A.: Capillary conduction of liquids through porous mediums. *Physics*, 1(5), 318-333, 1931.

617 Righes, A. A.: Water uptake and root distribution of soybeans, grain sorghum and corn. *Retrospective Theses and*
618 *Dissertations*. Iowa State University, 1980.

619 Roche, M.: Tracage naturel salin et isotopique des eaux du systeme du Lac Tchad, These de Doctorat d'Etat, Travaux et
620 Documents de l'ORSTOM, ORSTOM (Office de la Recherche Scientifique et Technique d'Outre-Mer) editions, Paris, 1980.

621 Scanlon, B. R., Keese, K. E., Flint, A. L., Flint, L. E., Gaye, C. B., Edmunds, W. M., Simmers. I.: Global synthesis of
622 groundwater recharge in semiarid and arid regions. *Hydrol. Process.* 20, 3335-3370, 2006.

623 Schaap, M. G., Leij, F. J., van Genuchten, M. T.: ROSETTA: a computer program for estimating soil hydraulic parameters
624 with hierarchical pedotransfer functions, *Journal of Hydrology*, 251, 163-176, 2001.

625 Schenk, H. J., Jackson, R. B.: Rooting depths, lateral root spreads and belowground aboveground allometries of plants in water
626 limited ecosystems. *Journal of Ecology*, 90, 480–494. <https://doi.org/10.1046/j.1365-2745.2002.00682.x>, 2002.

627 Shahrokhnia, M. H., Sepaskhah, A. R.: Single and dual crop coefficients and crop evapotranspiration for wheat and maize in
628 a semi-arid region. *Theoretical and Applied Climatology*, 114(3–4), 495–510. <https://doi.org/10.1007/s00704-013-0848-6>,
629 2013.

630 Šimůnek, J., Sejna, M., Saito, H., Sakai, M., van Genuchten, M. T.: The HYDRUS-1D software package for simulating the
631 one-dimensional movement of water, heat, and multiple solutes in variably-saturated media, Version 4.15, Riverside,
632 California, 2009.

633 Šimůnek, J., Šejna, M., van Genuchten, M. T.: *The HYDRUS Software Package for Simulating the Two- and Three-*
634 *Dimensional Movement of Water, Heat, and Multiple Solutes in Variably-Saturated Media*. Prague, 2011.

635 Sprenger, M., Volkmann, T. H. M., Blume, T., Weiler, M.: Estimating flow and transport parameters in the unsaturated zone
636 with pore water stable isotopes, *Hydrol. Earth Syst. Sci.*, 19(6), 2617-2635. <https://doi.org/10.5197/hess-19-2617-2015>, 2015.

637 Stumpp, C., Nützmann, G., Maciejewski, S., Maloszewski, P.: A comparative modeling study of a dual tracer experiment in a
638 large lysimeter under atmospheric conditions, *Journal of Hydrology*, 375, 566-577, 2009.

639 Stumpp, C., Stichler, W., Kandolf, M., Šimůnek, J.: Effects of land cover and fertilization method on water flow and solute
640 transport in five lysimeters: a long-term study using stable water isotopes, *Vadose Zone Journal*, 11(1).
641 <https://doi.org/10.2136/vzj2012.0075>, 2012.

642 ter Braak, C.J.F., Vrugt, J.A.: Differential Evolution Markov Chain with snooker updater and fewer chains. *Stat. Comput.* 18,
643 435–446. <https://doi.org/10.1007/s11222-008-9104-9>, 2008.

644 Tewelde, D. O.: Investigating unsaturated zone water transport processes by means of biogeochemical analysis of soil depth
645 profiles: a comparative study of two semi-arid sites. M.Sc.-Thesis, Leibniz Universitaet Hannover, 2017.

646 Tewelde, D. O., Koeniger, P., Beyer, M., Neukum, C., Gröschke, M., Ronnelngar, M., Rieckh, H., Vassolo, S.: Soil water
647 balance in the Lake Chad Basin using stable water isotope and chloride of soil profiles. *Isot. Environ. Health Stud.* 55, 459-
648 477. <https://doi.org/10.1080/10256016.2019.1647194>, 2019.

649 Tong, G. D., Liu, H. L., Li, F. H.: Evaluation of dual crop coefficient approach on evapotranspiration calculation of cherry
650 trees. *International Journal of Agricultural and Biological Engineering*, 9(3), 29–39.
651 <https://doi.org/10.3965/j.ijabe.20160903.1886>, 2016.

652 Vanderborght, J., Vereecken, H.: Review of dispersivity for transport modeling in soils, *Vadose Zone Journal*, 6(1), 29-52,
653 <https://doi.org/20.2136/vzj2006.0096>, 2007.

654 van Genuchten, M. T.: A close-form equation for predicting the hydraulic conductivity of unsaturated soils 1, *Soil Science*
655 *Society of America Journal*, 8(44), 892-898, 1980.

656 van Looy, K., Bouma, J., Herbst, M., Koestel, J., Minasny, B., Mishra, U., Montzka, C., Nemes, A., Pachepsky, Y. A.,
657 Padarian, J., Schaap, M. G.: Pedotransfer functions in earth system science: challenges and perspectives, *Reviews of*
658 *Geophysics*, 55(4), 1199-1256. <https://doi.org/10.1002/2017RG000581>, 2017.

659 Vaquero, G., Siavashani, N.S., García-Martínez, D., Elorza, J., Bila, M., Candela, L., Serrat-Capdevila, A.: The Lake Chad
660 transboundary aquifer. Estimation of groundwater fluxes through international borders from regional numerical modelling.
661 *Journal of Hydrology: Regional Studies*, 38 p. <https://doi.org/10.1016/j.ejrh.2021.100935>, 2021.

662 Vassolo, S.: The aquifer recharge and storage systems to reduce the high level of evapotranspiration. In: *Adaptive Water*
663 *Management in the Lake Chad Basin*. World Water Week 09, FAO, pp. 30-44, 2009.

664 Vereecken, H., Javaux, M., Weynants, M., Pachepsky, Y. A., Schaap, M. G., van Genuchten M. T.: Using pedotransfer
665 functions to estimate the van Genuchten-Mualem soil hydraulic properties: A review, *Vadose zone Journal*, 9(4), 759-820.
666 <https://doi.org/10.2136/vzj2010.0045>, 2010.

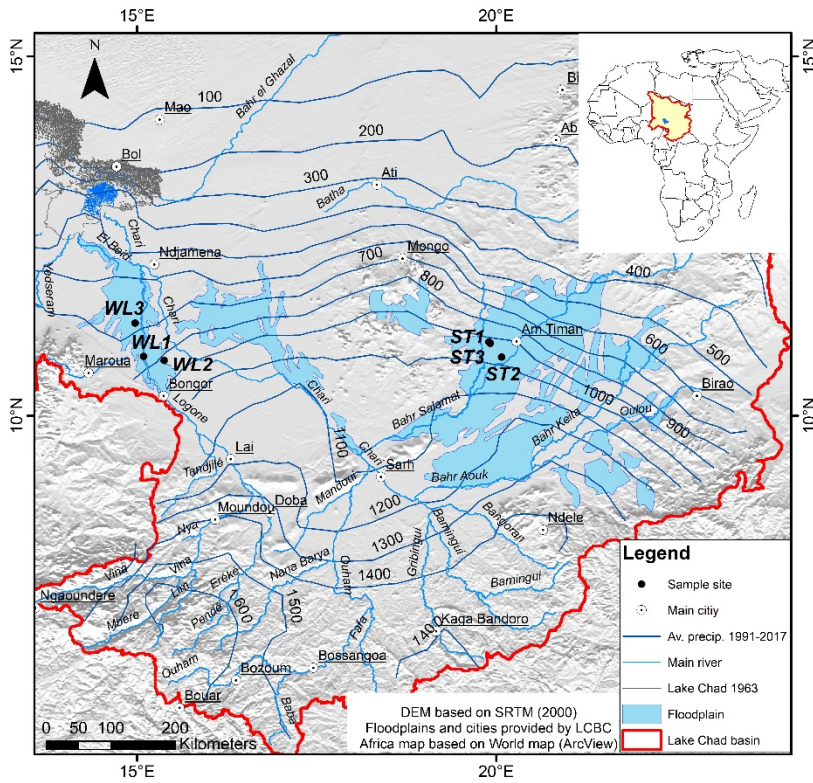
667 Vereecken, H., Schnepf, A., Hopmans, J. W., Javaux, M., Or, D., Roose, T., ... Young, I. M.: Modeling soil processes: Review,
668 key challenges, and new perspectives, *Vadose Zone Journal*, 15(5), 1-57. <https://doi.org/10.2136/vzj.2015.09.0131>, 2016.

669 Vieira, P. V. D., de Freitas, P. S. L., Ribeiro da Silva, A. L. B., Hashiguti, H. T., Rezende, R. Junior, C. A. F.: Determination
670 of wheat crop coefficient (K_c) and soil water evaporation (K_e) in Maringa, PR, Brazil, *African Journal of Agricultural*, 11(44),
671 4551–4558. <https://doi.org/10.5897/AJAR2016.11377>, 2016.

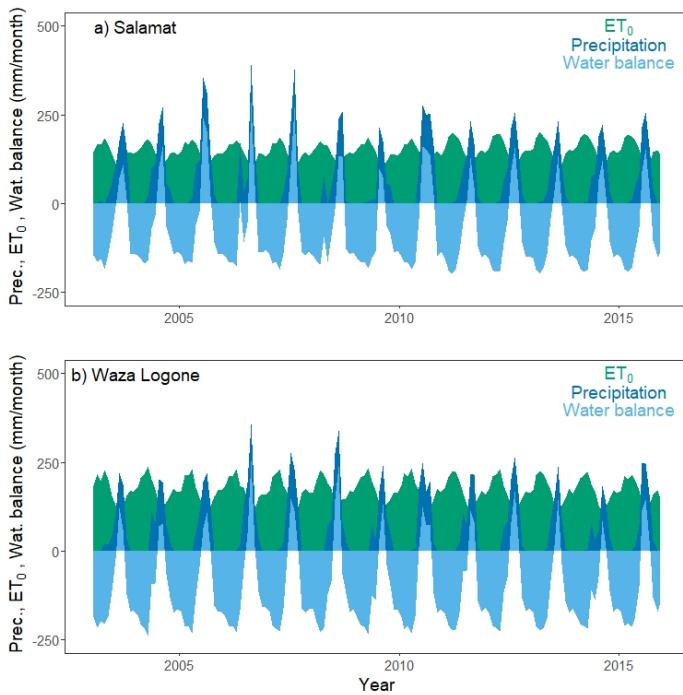
672 Vuillaume, G.: Bilan hydrologique mensuel et modélisation sommaire du régime hydrologique du lac Tchad, *Cahiers*
673 *ORSTOM. Série Hydrologie*, 18, 23–72, 1981.

674 Wu, Y., Du, T., Ding, R., Tong, L., Li, S.: Multiple Methods to Partition Evapotranspiration in a Maize Field. *Journal of*
675 *Hydrometeorology*, 139–149. <https://doi.org/10.1175/JHM-D-16-0138.1>, 2016.

676 Zairi, R.: Étude géochimique et hydrodynamique du Bassin du Lac Tchad (la nappe phréatique dans les régions du Kadzell
677 (Niger oriental) et du Bornou (Nord-Est du Nigéria)), PhD thesis, Université de Montpellier 2, Montpellier, 2008.
678



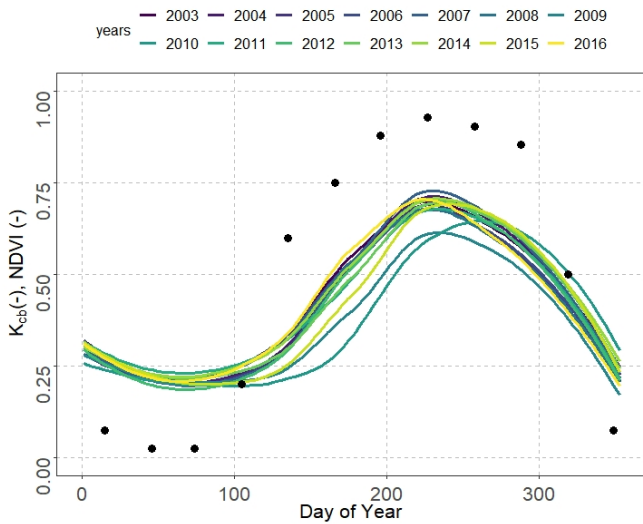
679
680 **Figure 1: Location of the six soil sampling sites within the Logone and Salamat river basins in the Lake Chad catchment. The map**
681 **inset shows the location of the Lake Chad basin in Africa.**



682

683 **Figure 2: Monthly precipitation, reference evapotranspiration from the CRUTS 4 database (NCAR, 2017) and derived water balance**
 684 **for Salamat and Waza Logone.**

685

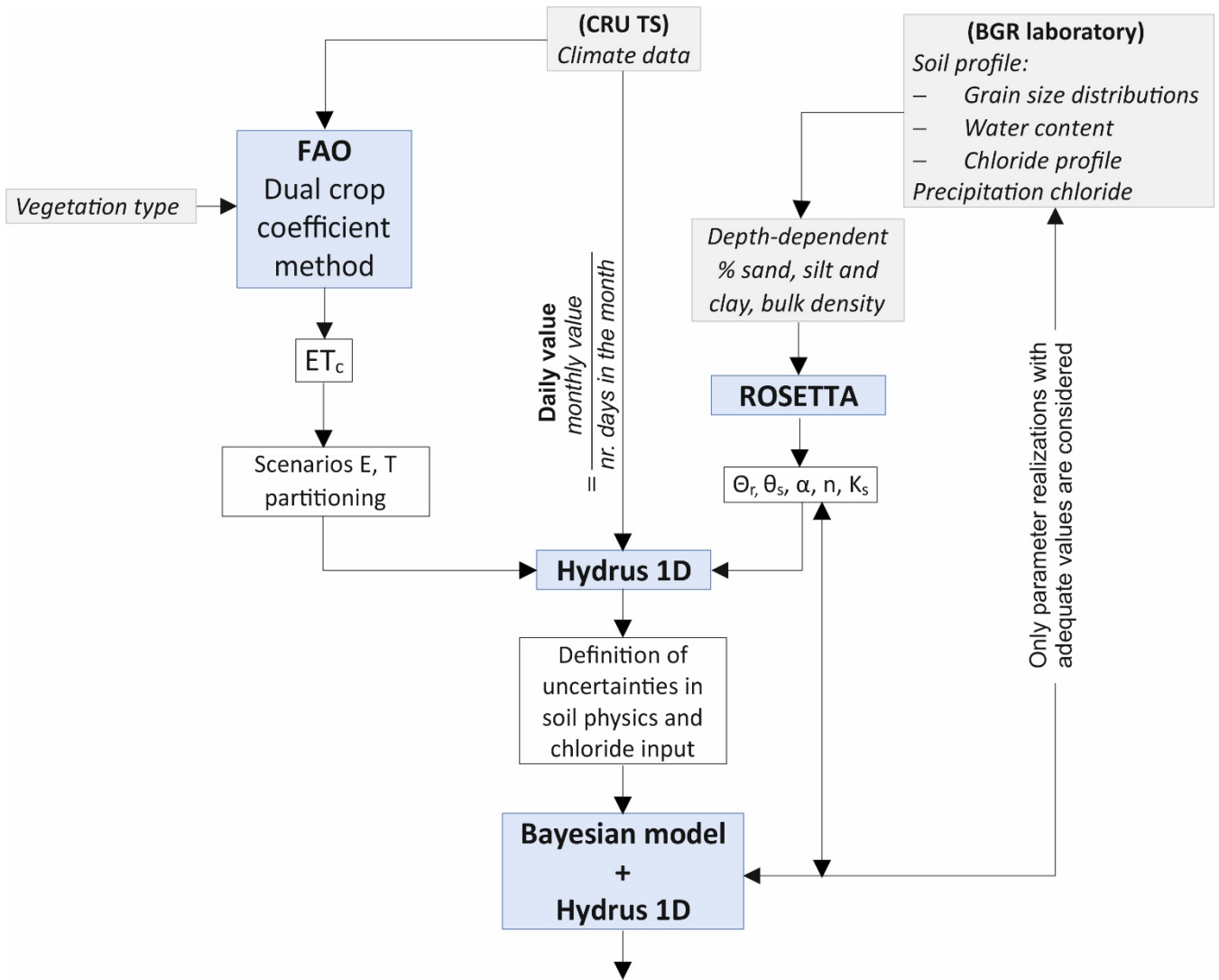


686

687 **Figure 3: Average Normalized Difference Vegetation Index (NDVI, MODIS 16 day interval and 250 m spatial resolution) measured**
 688 **between 2003 and 2016 in the Salamat region and estimated monthly basal crop coefficient (K_{cb} , black points) for location S3.**

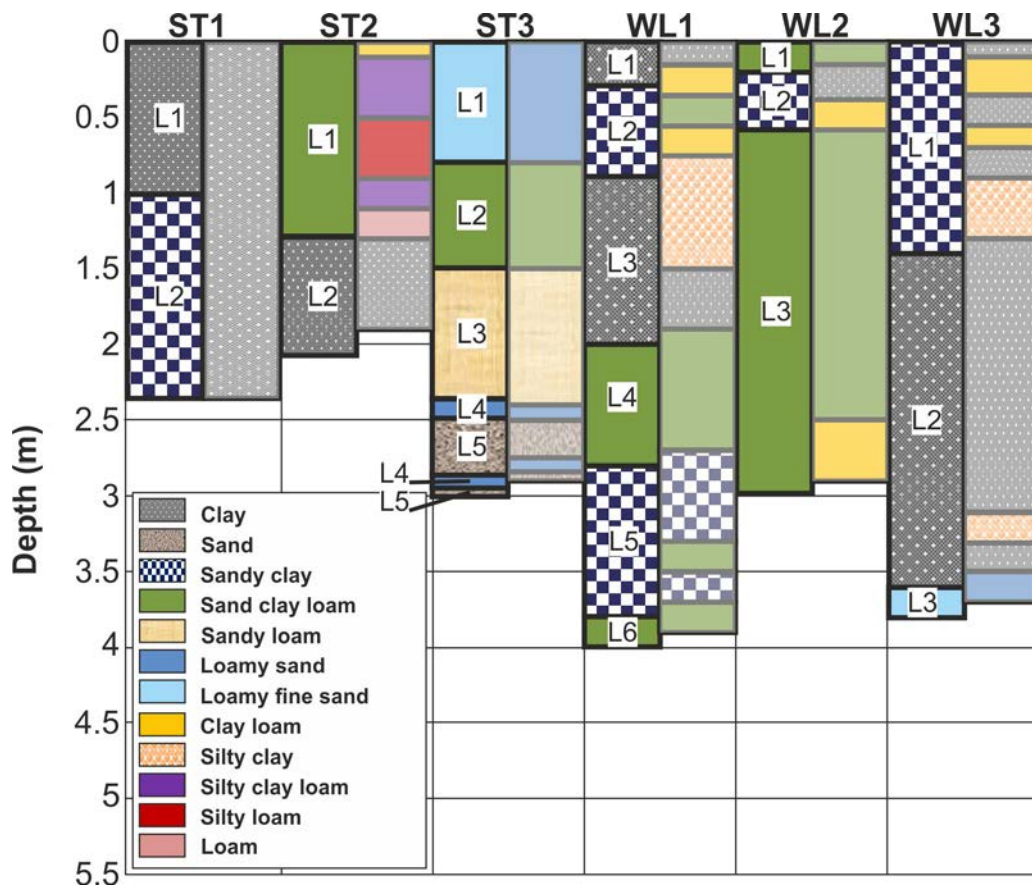
689

690



691

692 **Figure 4: Workflow of the modelling activities**

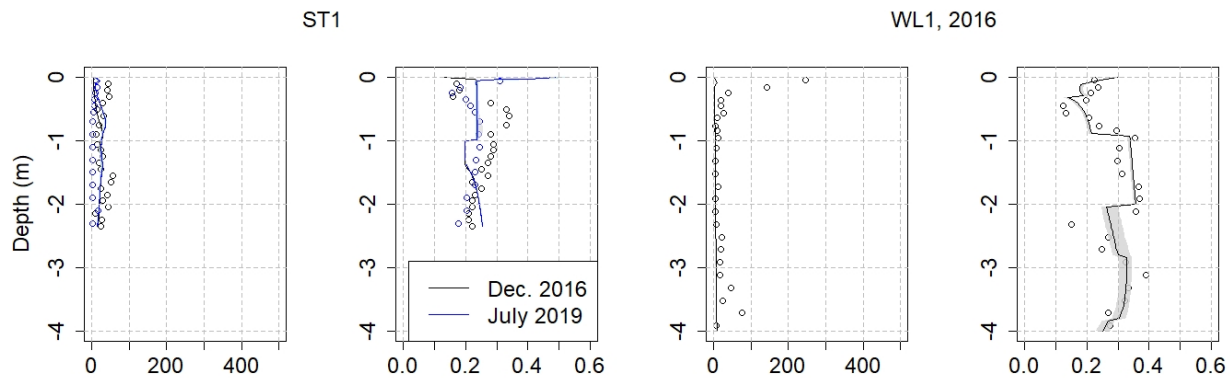


693

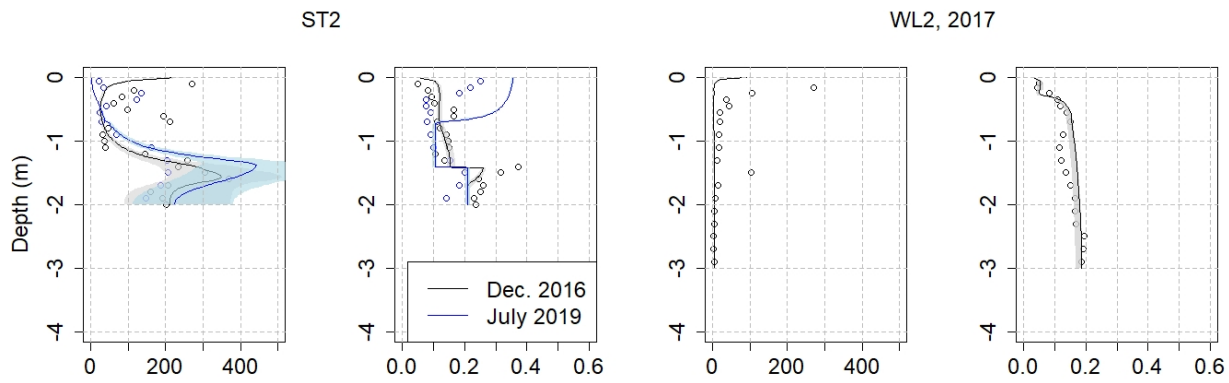
694

695

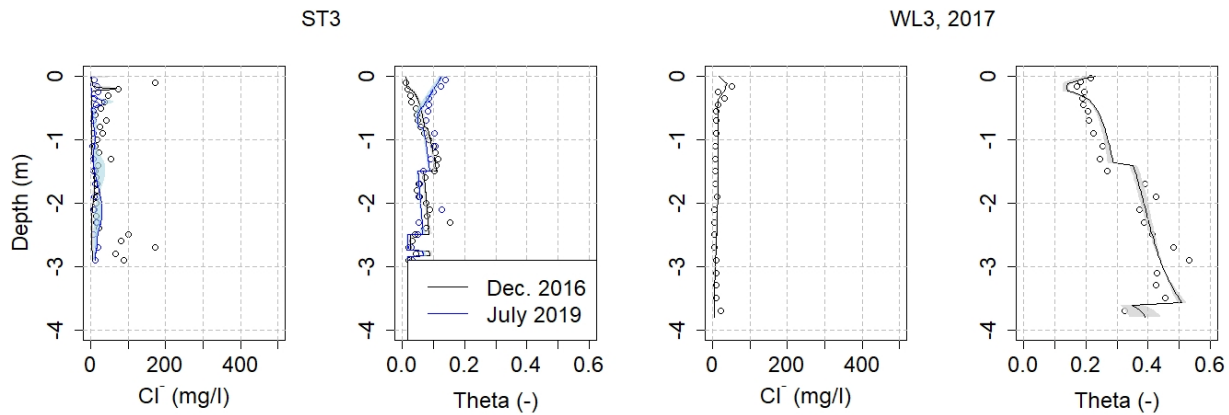
Figure 5: Soil textures used in the model (left column) defined according to the grain size distribution analysis (right column) for each of the six soil profiles.



696



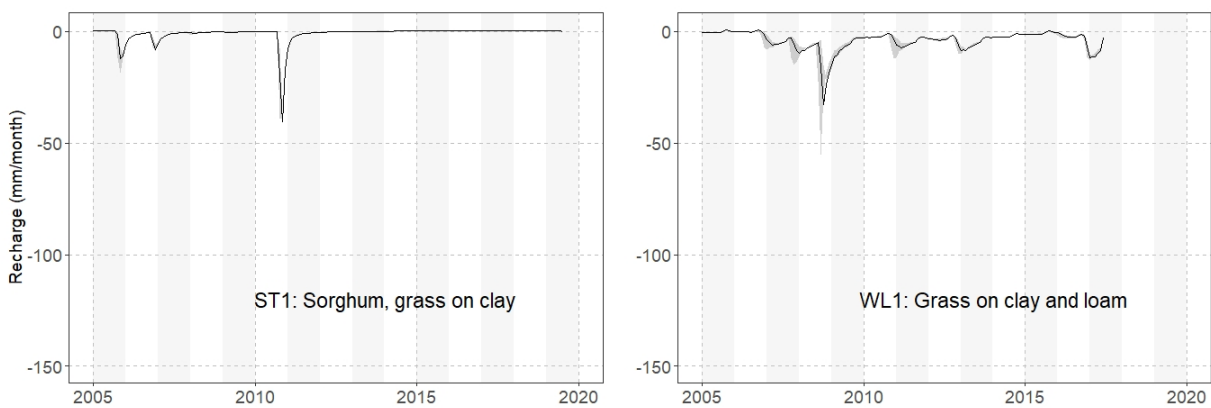
697



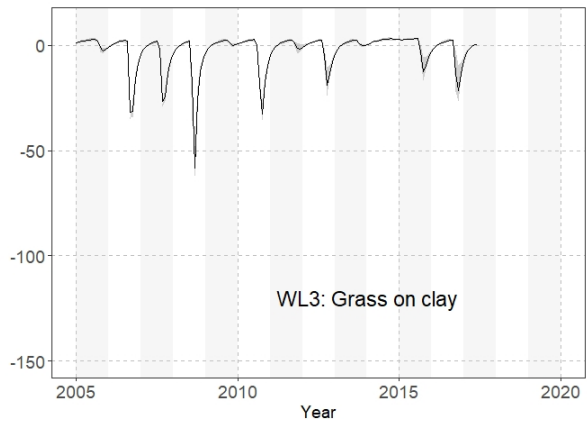
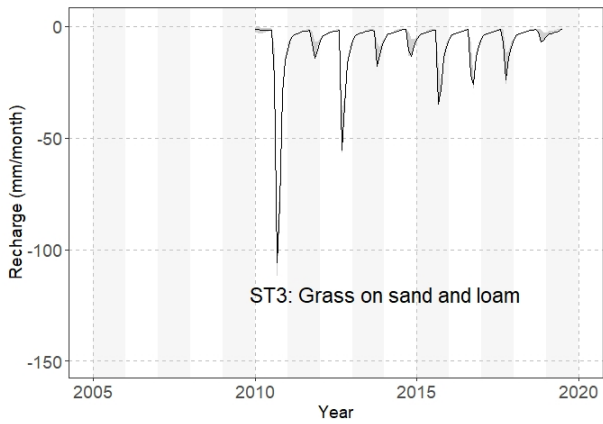
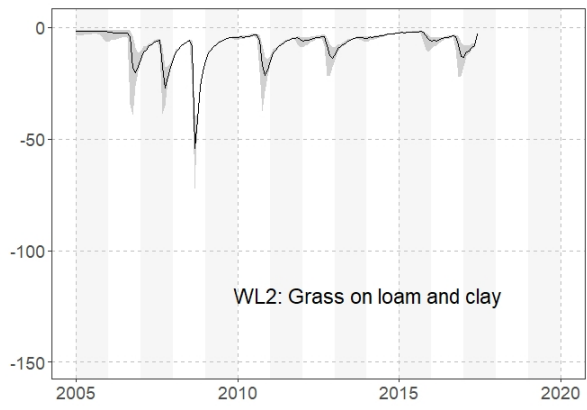
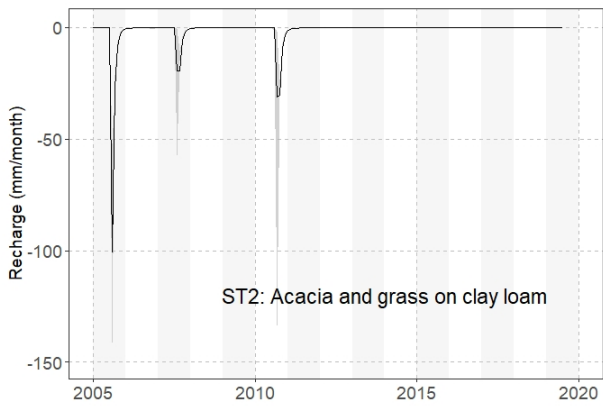
698

699 **Figure 6: Measured and simulated scenarios of chloride concentration and water content for all six soil profiles. Shaded areas**
 700 **represent the standard deviation of 100 randomly selected model runs.**

701



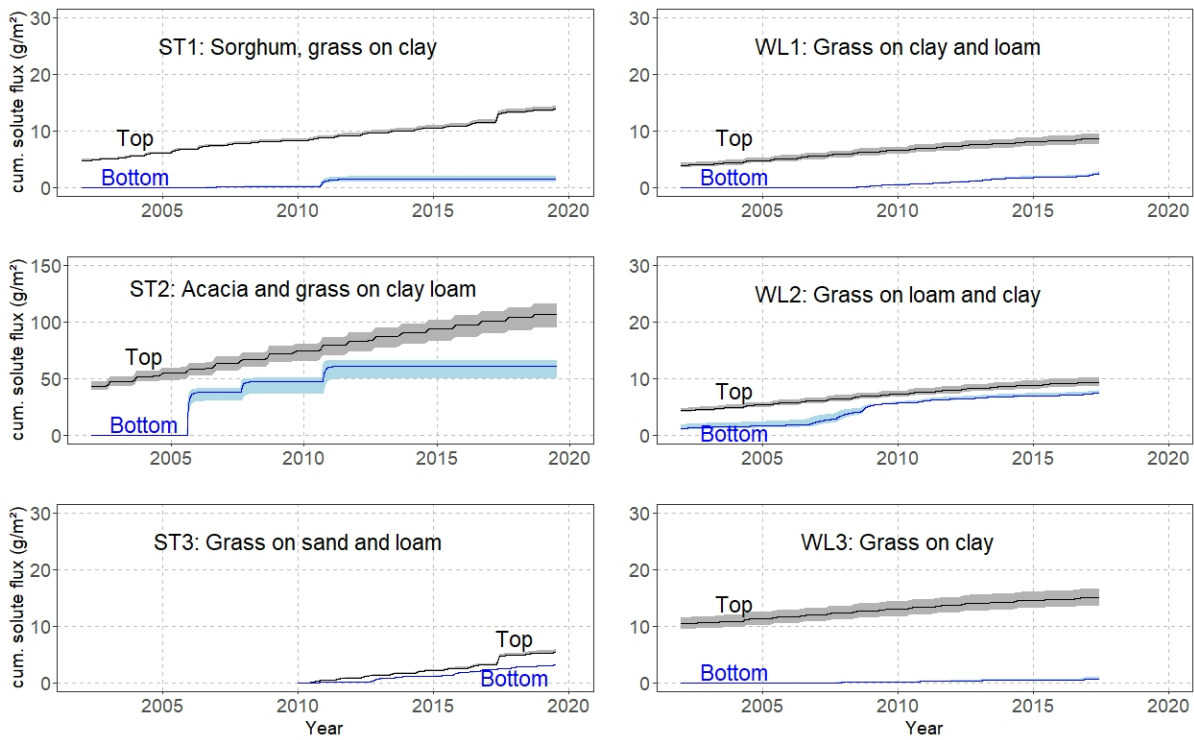
702



703

704

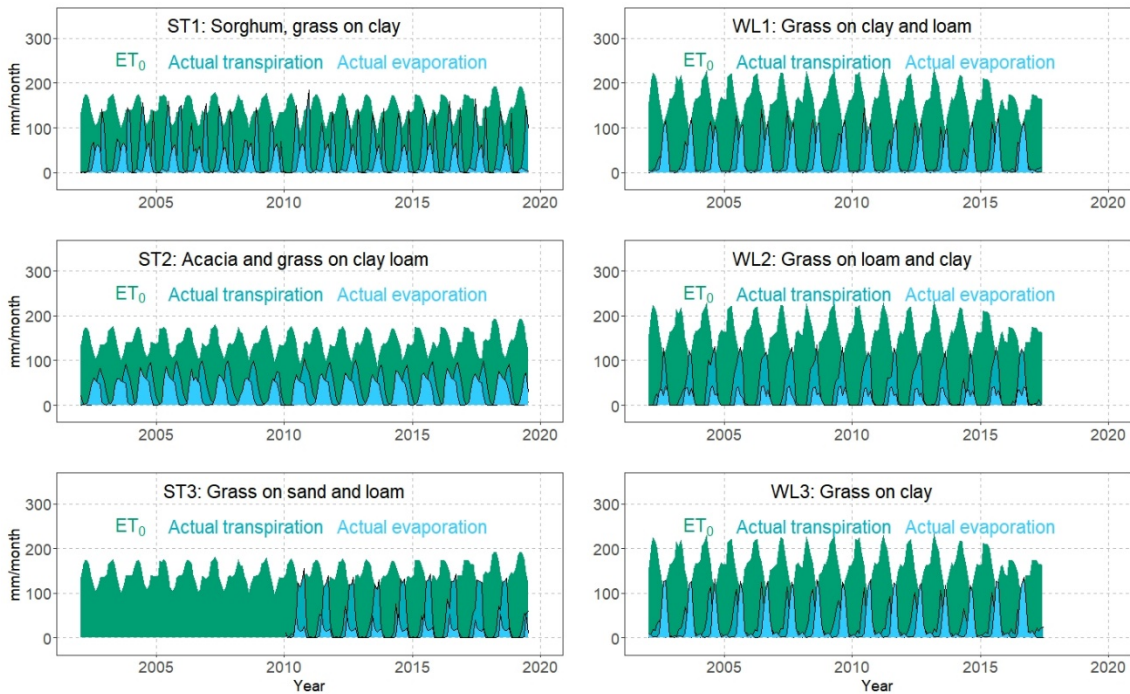
705 **Figure 7: Calculated groundwater recharge for all scenarios and sampling locations with indication of vegetation and soil texture.**



706

707 **Fig. 8: Cumulative solute flux on the upper and lower boundary of the models. The shaded areas represent the standard deviation**
 708 **of 100 randomly selected model runs. Note the different y-axis scales between sites.**

709



710

711 **Fig. 9: Reference evapotranspiration from the CRUTS 4 database (NCAR 2017) as well as modelled average actual evaporation and**
 712 **transpiration of 100 randomly selected model runs.**

713

714 **Table 1: Names and geographic coordinates of the sampling locations with average depths to groundwater.**

Name	Location	Date of Sampling	Drilling depth (m)	Longitude (°)	Latitude (°)	Elevation (m a.s.l.)	Depth to Groundwater (m)
ST1	Gos	07-12-2016	2.35	19.89644	11.02582	418	11
	Djarat	11-07-2019	5.0				
ST2	Kach	09-12-2016	2.0	20.07473	10.81649	396	16-18
	Kacha	16-07-2019	5.0				
ST3	Gos	11-12-2016	2.2	19.91687	11.00629	418	21
	Djarat	13-07-2019	5.0				
WL1	Katoa	01-06-2017	4.0	15.09235	10.82508	362	4
WL2	Loutou	01-06-2017	3.0	15.37817	10.76805	325	11-12
WL3	Zina	08-06-2017	3.8	14.97363	11.28858	304	3.6

715

716 **Table 2: Crop evapotranspiration scenarios used with the individual soil profiles.**

Scenario	K_{cb}	K_e	Root depth	Profile
Mean	average	average	average	All profiles
Min	minimum	minimum	average	All profiles
Min-RD	minimum	minimum	minimum	WL1
Mix-1	minimum	average	average	All profiles
Mix-2	average	minimum	average	ST1, WL2, WL3
Mix-3	maximum	average	average	ST3
Max	maximum	maximum	average	All profiles

717

718 **Table 3: Parametrization of water retention and unsaturated hydraulic conductivity functions according the Mualem-van**
719 **Genuchten model after Bayesian model calibration.**

Location	Texture	Depth (m)	θ_r (-)	θ_s (-)	α (m^{-1})	n (-)	k_s (md^{-1})
ST1	Clay	0-1	0.001	0.61 ± 0.01	2.13 ± 0.27	1.164 ± 0.008	0.09 ± 0.14
	Sandy clay	1-2.35	0.04	0.43 ± 0.03	2.63 ± 0.37	1.150 ± 0.011	0.43 ± 0.39
ST2	Sandy clay loam	0-1.4	0.04	0.38 ± 0.02	1.18 ± 0.08	1.36 ± 0.047	0.03 ± 0.16
	Clay	1.4 -2.1	0.07	0.48 ± 0.08	2.66 ± 0.36	1.203 ± 0.052	0.11 ± 0.28
ST3	Loamy fine sand	0-0.8	0.01	0.45 ± 0.08	3.69 ± 0.08	2.332 ± 0.196	2.96 ± 5.72
	Sandy clay loam	0.8-1.5	0.043	0.38 ± 0.07	2.81 ± 0.43	2.210 ± 0.172	2.44 ± 4.19
	Sandy loam	1.5-2.4	0.02	0.43 ± 0.08	3.44 ± 0.51	2.469 ± 0.330	1.66 ± 2.84
	Loamy sand	2.4-2.5	0	0.35 ± 0.06	3.77 ± 0.53	1.980 ± 0.265	2.03 ± 3.11
	Sand	2.5-2.75	0	0.34 ± 0.04	3.73 ± 0.53	2.730 ± 0.372	5.42 ± 8.86
	Loamy sand	2.75-2.84	0	0.35 ± 0.06	3.77 ± 0.53	1.980 ± 0.265	2.03 ± 3.11
	Sand	2.84-2.9	0	0.34 ± 0.04	3.73 ± 0.53	2.730 ± 0.372	5.42 ± 8.86
WL1	Clay	0-0.3	0.065	0.56 ± 0.09	1.37 ± 0.19	1.293 ± 0.092	0.17 ± 0.26
	Sandy clay	0.3-0.9	0.06	0.44 ± 0.07	2.85 ± 0.36	1.416 ± 0.125	0.21 ± 0.38
	Clay	0.9-2.0	0.103	0.42 ± 0.03	1.55 ± 0.21	1.187 ± 0.065	0.19 ± 0.42
	Sandy clay loam	2.0-2.8	0.075	0.49 ± 0.07	2.34 ± 0.33	1.598 ± 0.227	0.13 ± 0.28
	Sandy clay	2.8-3.8	0.081	0.43 ± 0.06	2.60 ± 0.35	1.266 ± 0.134	0.09 ± 0.19

	Sandy clay loam	3.8-4.0	0.071	0.40±0.05	2.69±0.37	1.291±0.137	0.12±0.24
	Sandy clay loam	0-0.2	0.03	0.41±0.07	3.22±0.45	1.502±0.151	0.30±0.57
WL2	Sandy clay	0.2-0.6	0.01	0.37±0.06	2.56±0.39	1.422±0.081	0.09±0.19
	Sandy clay loam	0.6-3.0	0.01	0.37±0.03	1.39±0.19	1.566±0.06	0.10±0.10
	Sandy clay	0-1.4	0.09	0.49±0.09	1.27±0.15	1.470±0.111	0.22±0.14
WL3	Clay	1.4-3.6	0.105	0.53±0.05	2.03±0.29	1.285±0.100	0.17±0.36
	Loamy fine sand	3.6-3.8	0.056	0.39±0.08	2.90±0.45	1.789±0.293	1.23±2.40

720

721 **Table 4: Average root mean square error (RMSE) and related standard deviation (SD) over all scenarios for water content (Theta)**
722 **and chloride concentration.**

Location, Year	Theta (cm ³ cm ⁻³)			Chloride concentration (mg l ⁻¹)		
	Average observation	Average simulation	Average RMSE	Average observation	Average simulation	Average RMSE
ST1, 2016/2019	0.25/0.22	0.23/0.23	0.06/0.04	30/6	18/22	19/19
ST2, 2016/2019	0.17/0.14	0.16/0.15	0.06/0.04	162/106	132/229	82/116
ST3, 2016/2019	0.06/0.08	0.07/0.06	0.02/0.02	42/10	6/13	58/10
WL1, 2017	0.27	0.27	0.05	31	6	59
WL2, 2017	0.13	0.15	0.02	40	3	117
WL3, 2017	0.31	0.33	0.04	12	13	9

723

724 **Table 5: Calculated average annual recharge, fraction of recharge on average annual precipitation, standard deviations of recharge**
725 **across the time-period 2005-2019 and 2005 – 2016 for Salamat and Waza Logone, respectively.**

Location	Average annual recharge (mm)	Fraction of average annual precipitation (%)	Standard deviation of annual recharge (mm)
ST1	7	0.9	17
ST2	9	1	29
ST3	93	12	69
WL1	28	4	32
WL2	54	8	46
WL3	6	1	48

726 **Table 6: Calculated average annual evaporation and transpiration and related standard deviations of 100 randomly accepted model**
 727 **runs.**

Location	Average annual evaporation (mm)	Standard deviation of evaporation (mm)	Average annual transpiration (mm)	Standard deviations of transpiration (mm)	Average actual evapotranspiration (mm)
ST1	210	9	553	11	763
ST2	366	22	388	27	754
ST3	137	12	552	11	689
WL1	344	20	317	23	661
WL2	146	14	477	28	623
WL3	376	12	305	10	681

728